Polym. Bull. (2010) 65:787–805
DOI 10.1007/s00289-010-0273-2

ORIGINAL PAPER

Encapsulation of BSA in polylactic acid–hyperbranched polyglycerol conjugate nanoparticles: preparation, characterization, and release kinetics

Xiujun Gao · Xinge Zhang · Xuejiao Zhang · Cui Cheng · Zhen Wang · Chaoxing Li

Received: 26 November 2009 / Revised: 6 March 2010 / Accepted: 6 April 2010 /
Published online: 16 April 2010

Abstract Nanoparticles based on an amphiphilic copolymer with polylactic acid (PLA) grafted onto hyperbranched polyglycerol (HPG) were prepared by the use of BSA as a model protein. The characteristics of the nanoparticles were evaluated using particle size analyzer, transmission electron microscopy, and X-ray photoelectron spectroscopy. The secondary structure of BSA released from nanoparticles were analysed by circular dichroism experiments. Cell viability of nanoparticles was also evaluated by using NIH 3T3 cells. The mechanism of BSA release was studied by fitting experimental data to three model equations. Results indicated that BSA diffusion and the polymeric relaxation jointly governed the overall release process. The detailed analysis of BSA release was performed using the first-order kinetic model equation, which gave a good fit to the experimental release data. The influence of different copolymer structures and BSA loading capacities on release profiles were also evaluated for the potential of using nanoparticles as controlled release protein delivery systems.

Keywords Amphiphilic copolymer · Biocompatibility · Biomacromolecule · Kinetics · Mathematical model

Introduction

Recently, substantial research efforts have focused on formulating therapeutic agents in biodegradable and biocompatible vehicles for controlled release of

X. Gao · X. Zhang (✉) · X. Zhang · C. Cheng · Z. Wang · C. Li (✉)
Key Laboratory of Functional Polymer Materials of Ministry Education, Institute of Polymer Chemistry, Nankai University, Tianjin 300071, China
e-mail: zhangxinge@nankai.edu.cn

C. Li
e-mail: lcx@nankai.edu.cn

biomacromolecules [1]. Polylactic acid (PLA)-based nanoparticles are attractive macromolecular carriers because of their biocompatibility, biodegradability, and non-toxicity [2–5]. Hyperbranched polyglycerol (HPG) is a highly branched macromolecule that, because of its hydrophilicity, modifiable surface and lower viscosities, has attracted increasing attention [6]. Although HPG is irregularly shaped and not perfectly symmetrical like dendrimers, it can be prepared in a single, one-pot reaction [7]. During the last years, many star polymers with multifunctional core and a number of linear PLA arms had been synthesized and some had even been used as nanocarriers for encapsulating guest molecules [8, 9]. However, the synthesis of those multi-arm star block copolymers was using multifunctional initiators for the directly catalyzed polymerization of hydrophobic monomers. Furthermore, in these amphiphilic architectures, the core was hydrophilic and the shell was hydrophobic. Here, the PLA-functionalized HPG was prepared and physicochemically characterized with the prospect of its application as a controlled protein delivery system.

However, difficulty achieving desired release rate is an important limitation in controlled protein delivery. Many factors, as the copolymer structure and loading capacity, have significant effects on the protein release mechanism [10], which can potentially be varied to design a controlled protein delivery system with desired release profiles. A great amount of work has gone into mathematical modeling to predict protein release characteristics or to provide insight into the fundamental processes that govern the release profile of biomacromolecules [11–15]. Once the mathematical models validate with experimental data, it may be helpful to manufacture a controlled drug delivery system with specified drug release profile. Therefore, it is necessary to derive a mathematical model suitable for establishing a quantitative relationship between the formulation variables.

In the work, BSA-loaded nanoparticles were prepared by nanoprecipitation method and the release profiles of the protein from nanoparticles with different copolymer structures and loading capacities were investigated. Based on the experimental results, mathematical models were proposed to predict protein release mechanism from nanoparticle populations. With the aid of different parameters from the most appropriate model, the release of the protein was discussed in detail. The results obtained lead us to the conclusion that hyperbranched polyglycerol–polylactic acid (HPG–PLA) nanoparticles can be successfully used as a carrier for controlled release of biomacromolecules.

Experimental

Materials

PLA with different molecular weights (12, 21, 40 and 60 kDa) were purchased from Shenzhen Bright China Industrial Co., Ltd. (Shenzhen, China). Glycidol was bought from Shenyang Gold Jyouki Technology Co., Ltd. (Shenyang, China). *N*,*N*'-Dicyclohexycarbodiimide (DCC) and 1-hydroxybenzotrizole (HOBt) were purchased from J&K-Acros Chemical Ltd. without further purification. *N*,*N*-dimethylformamide

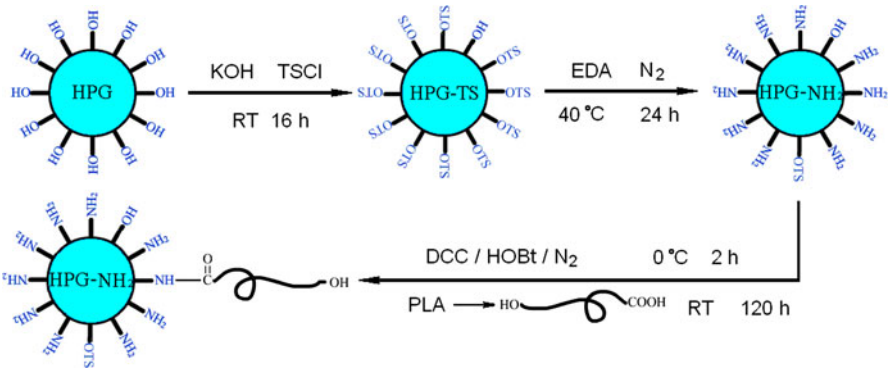

Fig. 1 Synthesis route of HPG–PLA

(DMF) and 1,2-ethylenediamine (EDA) were freshly distilled with anhydrous magnesium sulfate and sodium sulfate, respectively. BSA was obtained from Junyao Weiye Biochemical Co., Ltd. (Peking, China). All other chemicals were of analytical grade.

Synthesis and characterization of the copolymers

HPG was prepared by the anionic polymerization of glycidol in the presence of alkoxides [7]. The number average molecular weight of the product was about 6 kDa, which was measured by gel permeation chromatography (GPC) using a Viscotek system (Viscotek, USA). The Guinier radius of HPG was measured by small angle X-ray scattering method (SAXS) and performed using SAXS equipment (Bruker Nanostar). The amphiphilic copolymers were synthesized by a typical coupling reaction of PLA chains onto amino-modified HPG (HPG–NH_2) in the existence of coupling agents DCC and HOBt in DMF as shown in Fig. 1. Take the synthesis of HPG–PLA21 (with the molecular weight of PLA 21 kDa, PLA21 for short) for example, briefly, DCC (0.4 mmol) and HOBT (0.4 mmol) were added to 50 mL cooled DMF solution (0 °C) of PLA21 (0.2 mmol). HPG–NH_2 (0.6 mmol) was added portion-wise to the above solution. The solution was stirred at 0 °C for another 2 h, then the mixture was warmed up to room temperature and continued stirring under N_2 for 5 days, and then solid dicyclohexylurea (DCU) by-product was filtered out. The filtrate was diluted with DMF to the product concentration of around 1% and then fractioned with deionized water carefully. The second fraction was regarded as the principal component of the product (HPG–PLA21) [10, 16, 17].

The molecular weights and the polydispersities of the copolymers were measured by GPC, using a Waters system (Waters, USA). The structure of the copolymer was confirmed by ^{1}H NMR and FTIR.

Design and characterization of the copolymer nanoparticles

Preparation of nanoparticles

Nanoparticles were prepared according to the nanoprecipitation (NP) method as described previously [17, 18]. Briefly, HPG–PLA was dissolved in 1.5 mL of DMF at the concentration of 5 mg/mL and a certain amount of BSA was dissolved in 24 mL purified water. Finally, HPG–PLA solution was added dropwise to the aqueous phase (BSA solution) under stirring for 5 h. The mixture solution was then transferred into a dialysis membrane (10 kDa cutoff), and dialyzed against 5000 mL of distilled water for 24 h at 4 °C. Nanoparticles were obtained by centrifugation at 20,000 rpm for 30 min, lyophilized overnight, and stored at 4 °C for further use.

Characterization of nanoparticles

Transmission electron microscopy (TEM) was performed on a Philips EM400ST to observe the morphologies of the copolymer nanoparticles. A drop of nanoparticles was placed onto a 200-mesh copper grid and allowed to equilibrate. After the deposition of nanoparticles, water was allowed to be removed with a filter paper from the grids at room temperature before loaded in the microscope.

A dynamic light scattering particle size analyzer (Brookhaven, INNDVO300/BI900AT) was used to determine the hydrodynamic radii and polydispersities of nanoparticles at 37 °C. The analysis was carried out with He–Ne laser light of fixed wavelength (636 nm) at 90° using samples appropriately diluted with filtered water. All samples were analyzed in triplicate.

The surface chemical compositions of freeze-dried nanoparticles (blank and BSA-loaded) were analyzed by X-ray photoelectron spectroscopy (XPS). The XPS measurements were performed on a PEKIN ELMER PHI 1 600 spectrometer using an Mg Kα X-ray source. All binding energies were referenced to the C1s hydrocarbon peak at 284.8 eV.

The zeta-potential of BSA-loaded nanoparticles was measured using a Zeta potential meter (Zetasizer 3 000HS, Brookhaven) at 37 °C. The samples were prepared with double distilled water to ensure low ionic strength. All samples were analyzed in triplicate.

Water uptake and residual mass experiments were carried out as follows: 20 mg nanoaparticles was dried to a constant weight in vacuo and immersed in phosphate buffer saline (PBS, 0.1 M, pH 7.4) at 37 °C. On the 4th day, the sample was taken out from PBS, washed rapidly with ethanol 95% and blotted off carefully in between sheets of tissue paper to remove the surface-adhered liquid [14]. And then the sample was weighed on an electronic microbalance (AE 240, Mettler, Switzerland) to an accuracy of ±0.01 mg. The percentage of equilibrium water uptake was calculated as follows:

$$\text{Water uptake } (\%) = (W_w - W_d)/W_d \times 100\% \quad (1)$$

where W_w was the weight of the wet sample, and W_d was the initial weight of the sample. Then, the sample was dried in vacuo to a constant weight. The residual mass was calculated according to the following formula:

$$\text{Residual mass } (\%) = W_c/W_i \times 100\% \quad (2)$$

where W_i and W_c represented the initial weight of the sample and that of constant weight after dried on the fourth day, respectively. All samples were analyzed in triplicate, and the error bars in the plot were the standard deviation.

The BSA loading capacity (LC) was measured according to the previous report [19] and calculated as follows:

$$\text{LC } (\%) = \frac{\text{The mass of total BSA} - \text{The mass of free BSA}}{\text{The mass of nanoparticles}} \times 100\% \quad (3)$$

the amount of free BSA in the supernatant was measured by the Bradford method using a UV spectrometer (Shimadzu UV-2550) at 595 nm [20]. All samples were analyzed in triplicate, and the error bars in the plot were the standard deviation.

Cell viability was evaluated by using NIH 3T3 cells. The cell line was cultured in Dulbecco's modified Eagle's medium (DMEM, pH 7.4) in a humidified atmosphere (5% CO_2/95% O_2). The cells were seeded into 96-well plates at 10,000 cells per well. The plates were then returned to the incubator, and the cells were allowed to grow to confluence for 72 h. The blank nanoparticle solutions were diluted with culture medium to give suitable concentrations for further use. Then the media in the wells were replaced with the pre-prepared culture medium–sample mixture (200 μL). The plates were then returned to the incubator and maintained in 5% CO_2 at 37 °C for 72 h. Each sample was tested using three replicates per plate. After incubation, the culture medium and 20 μL of MTT solution were used to replace the mixture in each well. The plates were then returned to the incubator and incubated for a further 4 h in 5% CO_2 at 37 °C. The culture medium and MTT were removed. Isopropanol (100 μL) was then added to each well to dissolve the formazane crystals. The plate was placed in 5% CO_2 at 37 °C for 10 min and for 15 min at 6 °C before measurement. The optical density was read on a microplate reader at 492 nm. Cell viability was determined as a percentage of the positive control. Cells untreated with the solution of blank nanoparticles were used as the positive control and their viability was set to 100%. Each experiment was performed in triplicate and the results were reported as mean standard deviation. The cell viability in each well was calculated as follows:

$$\text{Cell viability } (\%) = \frac{\text{Average optical density values in experimental groups}}{\text{Average optical density values in the control groups}} \times 100\% \quad (4)$$

Statistical data analysis was performed using the paired t test with SPSS statistical software (version 15.0). All tests were conducted with 95% confidence intervals and significant differences were identified when the level of significance was less than 0.05 ($p < 0.05$). Comparisons described as "no significant difference between groups" were based on a level of significance greater than 0.05 ($p > 0.05$).

Circular dichroism (CD) spectra were recorded on a Jasco-715 Spectropolarimeter (JASCO, Tokyo, Japan) at 37 °C under a constant flow of nitrogen gas. Typically a cell with a 1 mm path length was used for spectra recorded between 190 and 260 nm with sampling points every 0.1 nm. The spectra represented the average of 8–20 scans and CD intensities were expressed in mdeg.

In vitro protein release

Protein release studies were conducted with various HPG–PLA copolymer nanoparticles. 20 mg of protein-loaded nanoparticles was immersed in 5 mL of PBS (0.1 M, pH 7.4) and incubated at 37 °C under horizontal shaking. At predetermined time points, the sample was centrifuged at 20,000 rpm for 30 min. 100 μL supernatant was withdrawn and the sample was replenished by another 100 μL fresh buffer solution. The amount of free BSA in the 100 μL supernatant was determined by the Bradford method [21]. In each experiment, the sample was analyzed in triplicate and the error bars in the plot were the standard deviation.

Mathematical analysis of the protein release mechanism

In order to study BSA release mechanism from different molecularly designed HPG–PLA copolymers, three models were considered to fit the experimental release data.

Model 1 is described by the well-known Ritger–Peppas equation [22], which is a more comprehensive, but still very simple, semi-empirical equation:

$$M_t/M_\infty = K_{\mathrm{RP}} t^n \ (M_t/M_\infty \leq 60\%) \tag{5}$$

where M_t/M_∞ is the fractional drug release, K_{RP} is a constant indicating structural and geometric characteristics [15], t is the release time and n is the release exponent that is related to protein release mechanism. The equation can be seen as a generalization of the observation that superposition of two apparently independent mechanisms of drug transport, a Fickian diffusion and a case-II transport [23]. For spherical matrices, when $n \leq 0.43$, the protein release mechanism was Fickian diffusion. When $n > 0.85$, super case II type of drug release occurred. When the value of n was between 0.43 and 0.85, non-Fick (anomalous) release was observed [24].

Model 2 was proposed by Peppas–Sahlin equation [25]:

$$M_t/M_\infty = K_1 t^{0.5} + K_2 t \ (M_t/M_\infty \leq 95\%) \tag{6}$$

the first term represented the contribution of Fickian diffusion and the second term was the relaxational contribution.

Model 3 [26–28] could be expressed as follows:

$$M_t/M_\infty = a_1(1 - \exp(-k_1 t)) + a_2(1 - \exp(-k_2 t)) \tag{7}$$

where k_1 and k_2 were the first-order release rate constants, a_1 and a_2 meant the percentage of BSA located on the out layer and entrapped inside the nanoparticles, respectively. This model is appropriate for the protein release data here as described below.

To find out the models with different numbers of parameters that described the data properly, the adjusted coefficient of determination (R^2_{adjusted}) was obtained. It could be defined as:

$$R^2_{\text{adjusted}} = 1 - (n-1)\left(1 - R^2\right)/(n-p) \quad (8)$$

where n was the number of experimental data points, p was the number of parameters in the model and R^2 was the coefficient of determination. The model that best explained the data was the one that showed the highest adjusted coefficient of determination [29].

Results and discussion

Synthesis and characterization of the copolymers

The conjugation of the peptide or other amide bond has been intensively studied in recent years [30, 31]. The coupling reaction of the free amino group with the free carboxylic group could take place efficiently upon treatment with DCC [32, 33] as shown in Fig. 1.

In order to obtain the coupled product as one PLA chain grafting onto one HPG molecule, an excess of HPG–NH_2 should be used in the reaction. The characterization data of the copolymers are summarized in Table 1. GPC chromatography (Fig. 2) exhibited that only one GPC peak appeared and the polydispersity index of molecular weight remained to be equal or lesser than 1.6. This confirmed that one single PLA chain was coupled to a HPG molecule.

The structure of the block copolymer was characterized with ^{1}H NMR in DMSO. Methyl and methine protons of the PLA segments give peaks at 1.5 and 5.2 ppm, respectively. Peaks from 3.3 to 3.7 ppm are assigned to the protons on the methylene and methine groups of HPG [7].

The FTIR spectrum of HPG–PLA21 is shown in Fig. 3c as described previously [17]. The absorption at 1665 cm^{-1} is attributed to the stretching vibration of carbonyl C=O in the amide bond of the copolymer, while an absorption band at 1526 cm^{-1} is assigned to the N–H bending vibration of a secondary amide [34–36]. Typical absorptions of PLA can be found in Fig. 3c. The peak at 1759 cm^{-1} is assigned to the stretching of C=O in the terminal carboxyl and that at 3508 cm^{-1} to

Table 1 The copolymers prepared with HPG and PLA

Material	PLA (kDa)	Mn (kDa)	Mw/Mn	Yield (%)
HPG–PLA12	12	18	1.3	57
HPG–PLA21	21	27	1.4	53
HPG–PLA40	40	44	1.6	52
HPG–PLA60	60	65	1.3	63

The ratio of PLA to HPG (mol/mol) is 1:3. The number average molecular weight of HPG is about 6 kDa and Mw/Mn is about 2.27, the Guinier radius of HPG is about 4.5 nm

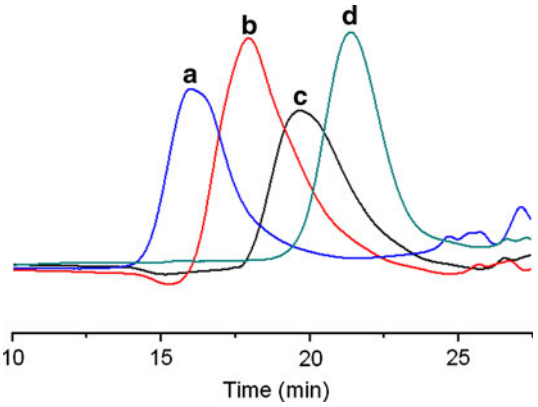

Fig. 2 Gel permeation chromatograms of the copolymers with different molecular weights. (*a*) HPG–PLA60, (*b*) HPG–PLA40, (*c*) HPG–PLA21, and (*d*) HPG–PLA12

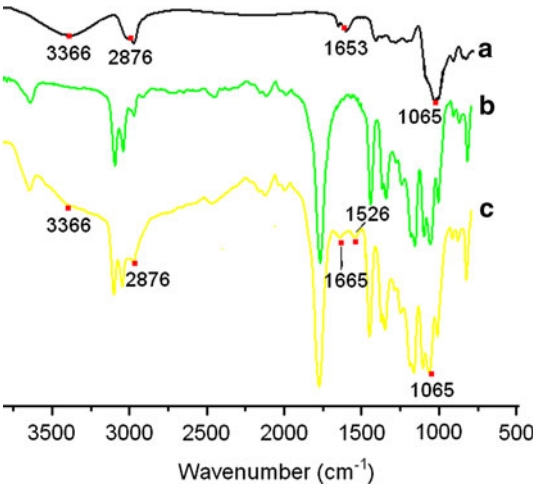

Fig. 3 FTIR spectra of (*a*) HPG alone, (*b*) PLA, and (*c*) HPG–PLA21

the terminal hydroxyl group. The absorptions at 1383 and 1455 cm^{-1} result from the bending of –CH–, while the peaks at 2945 and 2996 cm^{-1} are due to the stretching of –CH– and –CH3 [37]. Typical absorptions of HPG (Fig. 3a) can also be found in Fig. 3c. Absorption at 3366 cm^{-1} result from the stretching of –OH while peaks at 2876 cm^{-1} are due to the stretching of –CH–. The peak at 1065 cm^{-1} is due to the stretching vibration of C–O–C [17]. These results confirm that the copolymer is successfully synthesized.

Physicochemical characterization of HPG–PLA nanoparticles

Residual mass and water uptake

The experimental data of residual mass and water uptake of HPG–PLA nanoparticles are shown in Fig. 4. When HPG content increased from 9.4 to 33.3% in the copolymer, water uptake increased from 32 to 71%. Namely, when the content of

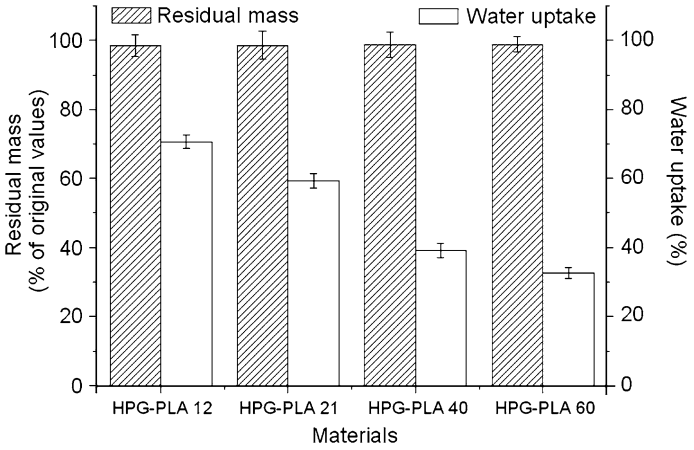

Fig. 4 Residual mass and water uptake of HPG–PLA in 4 days

HPG segment in the copolymer increased, the nanoparticles became more hydrophilic and could uptake more water. This may be induced by the introduction of hydrophilic hyperbranched HPG, which can bring more channels for water molecules to penetrate into the matrix. Such a hydrophilic character of the HPG–PLA can be helpful to preserve the stability of a protein after it is entrapped into the copolymer nanoparticles [38]. However, during the 4 days, no significant degradation could be observed for all samples. The degradation rate of PLA segment was quite low as shown in Fig. 4. It suggests that the protein release may not be an erosion control process.

Morphology of the nanoparticles

The morphology of the nanoparticles (HPG–PLA 21, *LC* is 12.3%) is shown by the TEM image in Fig. 5, which all present spherical shapes and no aggregation occurs among the nanoparticles. However, the diameter observed in TEM was a little smaller than that detected on the particle size analyzer (Table 2). Because the nanoparticles for the TEM observation were air-dried and those for the detection of the hydrodynamic diameter were in the aqueous medium, the outer water-solvated layer of the air-dried nanoparticles would be thinner so that the smaller diameter was displayed on the TEM [38].

XPS analysis and zeta-potential experiment

XPS is one of very powerful tools for understanding the content of elements and the adsorption of various corresponding materials on nanoparticles surface. The surface chemical compositions of blank (HPG–PLA 21) and BSA-loaded nanoparticles (HPG–PLA 21, *LC* is 12.3%) were analyzed by XPS. The chemical composition percent of sulfur on the surface of blank nanoparticles was 0%. However, 0.4% of sulfur atoms could be found on the surface of BSA-loaded nanoparticles. The

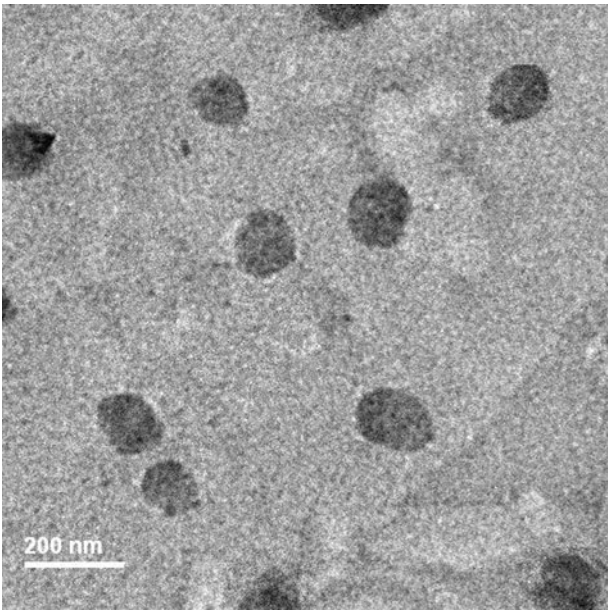

Fig. 5 TEM micrograph of BSA-loaded HPG–PLA21 nanoparticles

Table 2 The influence of processing factors on LC and particle size using nanoprecipitation technique

NPs made with	BSA used initially in aqueous phase (mg)	LC (%)	Average diameter (nm)	Polydispersity index
HPG–PLA12	0	–	128.3 ± 1.6	0.132
	5.0[a]	9.1 ± 0.6	163.3 ± 1.5	0.139
HPG–PLA21	0	–	151.4 ± 1.2	0.085
	1.0	4.6 ± 0.9	186.0 ± 2.0	0.143
	5.0[a]	12.3 ± 0.7	173.2 ± 1.3	0.094
	10.0	13.7 ± 1.2	167.8 ± 2.4	0.196
	20.0	13.9 ± 1.4	–	–
HPG–PLA40	0	–	187.9 ± 2.8	0.201
	5.0[a]	15.5 ± 1.1	204.2 ± 2.9	0.213
HPG–PLA60	0	–	263.5 ± 2.7	0.200
	5.0[a]	17.8 ± 1.3	287.4 ± 3.1	0.247

HPG–PLA used initially: 5 mg; aqueous phase: 8 mL; organic phase (DMF): 1 mL.

[a] 5 mg BSA was used initially in the aqueous phase and other conditions were the same as shown in Table 2

detection of 0.4% sulfur means that a portion of protein locate on the surface of nanoparticles, since sulfur atoms are typical atoms presented in BSA as –S–S– and free sulphydryl. XPS results reveal that there is some adsorption of BSA on the surface of nanoparticles.

The surface charge of blank nanoparticles (HPG–PLA 21) is positive (+20.75 ± 2.1 mV). The positive surface charge of blank nanoparticles is probably due to the ionization of HPG-NH_2 at the particle surface in aqueous solution. In the copolymer, hydrophilic segment HPG-NH_2, could exist in the ionic form of HPG–NH_3^+ in aqueous medium. However, the zeta potential value of BSA-loaded nanoparticles (HPG–PLA 21, LC is 12.3%) was about −24.23 ± 1.4 mV, which was close to that of BSA alone in aqueous solution (−26.49 ± 2.2 mV). This may be because the protein acts as a surfactant to stabilize the nanoparticles by acting as a steric barrier on the surface of nanoparticles. As a consequence, the absolute value of the zeta potential of BSA-loaded nanoparticles was high, which increased the corresponding electrostatic repulsion between the nanoparticles and was in favor of the stability of nanoparticles.

The particle size and LC of the nanoparticles

The particle size, polydispersity index, and LC data are shown in Table 2. Nanoparticles had a size in the range of 128 to 287 nm. The particle size decreased with decreasing molecular weight of the copolymers. The higher M_n of PLA segments contributed to the viscosity increase of copolymer solution, which could result in particle size increase [10]. At the same time, HPG–PLA with longer hydrophobic segment could effectively retard the leak of BSA through hydrophobic interactions, which was in favor of enhancing LC.

In order to investigate the effect of BSA concentration in the initial aqueous phase on particle size and LC, nanoparticles made with HPG–PLA21 were prepared with different BSA concentration in the initial aqueous phase (0.125, 0.625, 1.25 mg/mL). An increasing of BSA concentration from 0.125 to 1.25 mg/mL resulted in particle size decrease slightly. As a model protein, BSA can be absorbed on the surface of the nanoparticles, which has been demonstrated by XPS and zeta-potential experiments. So, the decrease of the particle size might result from the reduced collision frequency between droplets because of the electrostatic repulsion and steric hindrance effects of BSA on the surface of the nanoparticles. As expected, an increasing of BSA concentration induced LC increase. However, the increase in *LC* with BSA concentration in the aqueous phase does not seem to be linear. This may be because the more BSA has been already entrapped in the nanoparticles, the stronger diffusion drive there is to release them out. So, it would be more difficult to entrap added BSA into nanoparticles as an increasing of BSA concentration in the matrices.

Cell viability

Proteins can be deactivated by the hydrophobicity of PLA when they are encapsulated in the nanoparticles [10, 39]. Therefore, it was important in the present project to verify the innocuous nature of the copolymer nanoparticles. A series of experiments were performed to evaluate the potential toxicity of the HPG–PLA nanoparticles.

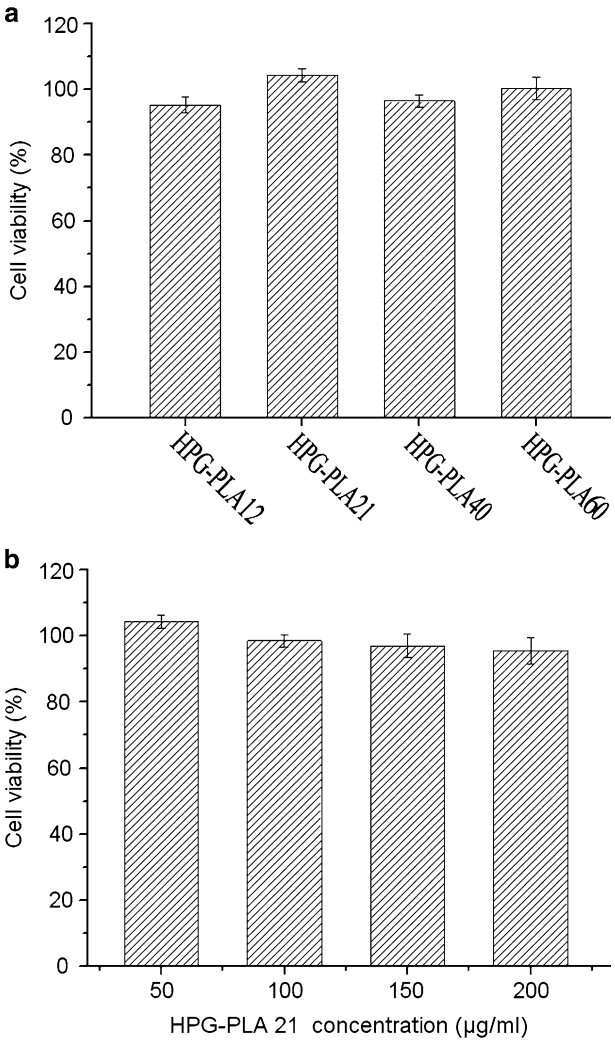

Fig. 6 **a** Cell viability assay in NIH 3T3 cell line treated with 50 μg/mL concentration of HPG–PLA12, HPG–PLA21, HPG–PLA40, and HPG–PLA60 nanoparticle solutions. **b** Various concentrations of HPG–PLA21 nanoparticles: 50, 100, 150 and 200 μg/mL. Cell viability was determined by the MTT assay and expressed as a percentage of control, that is, the untreated cells (100% of longitudinal coordinate)

Figure 6 shows the results of cytotoxicity measurements of the samples analyzed by the MTT method in the NIH 3T3 cell line. As shown in Fig. 6a, it was found that the cell viability of NIH 3T3 cells was maintained around 100% cultured with different copolymer nanoparticle solutions for 72 h. It was also found that the cell viability of NIH 3T3 cells was maintained over 90% with different concentrations of HPG–PLA21 nanoparticles solutions for 72 h (Fig. 6b) and no significant toxicity was showed with an increase of the concentration. Namely, the cytotoxicity is 0 or 1 grade according to the test standard of USP [40], meaning that the materials have no

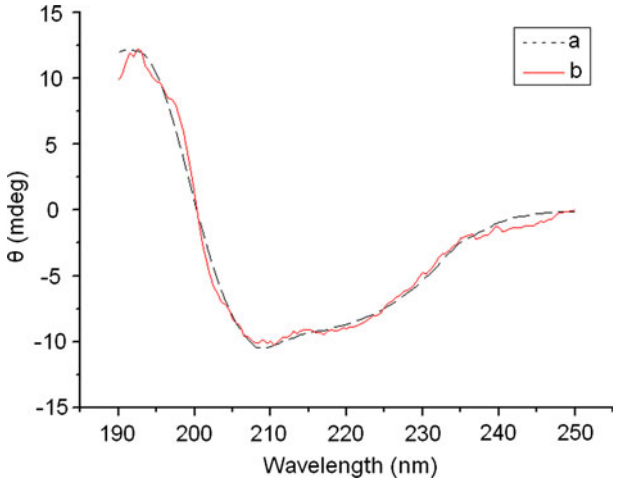

Fig. 7 Circular dichroism spectra of BSA solutions. (*a*) Native BSA; (*b*) BSA released from HPG–PLA21 nanoparticles after 4 days

cytotoxicity. There was no significant difference ($p > 0.05$) between control and test groups, which indicated that the blank nanoparticle solutions had no obvious effect on the cell viability. Therefore, the results suggest that the copolymer nanoparticles possess good biocompatibility and no cytotoxicity, they have high potential for in vivo use.

Circular dichroism spectra

The analysis of CD spectra can provide valuable information about the secondary structure of macromolecules. Figure 7 exhibits spectra characteristic standard BSA and BSA release from nanoparticles after 4 days. Two extreme valleys, respectively, at 220 and 208 nm were found in the CD spectrum of standard BSA, which suggested the existence of α-helical structures [41] in the standard BSA. The quantitative α-helix content analysis of BSA was estimated according to the equation used by other researchers [42]. It is measured that the native BSA in the PBS buffer solution (pH 7.4) has 59.8% of α-helix. The helix content of BSA released from HPG–PLA21 nanoparticles after 4 days is about 58.7%, which is similar with that of the native BSA. The strong double minima of BSA released from nanoparticles after 4 days at 220 and 208 nm occurred without significant difference from those of the native BSA. Thus, experimental evidence provides for the fact that BSA secondary structure has not been distorted.

Mathematical analysis of BSA release mechanism

The overall BSA release mechanism from HPG–PLA nanoparticles strongly depends on the design of protein delivery system, as the composition of the copolymer and the geometries of nanoparticles. There are many devices that exhibit

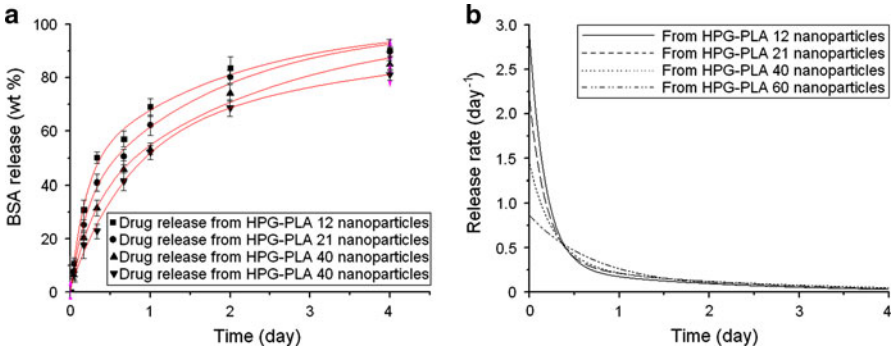

Fig. 8 **a** In vitro release profiles of BSA from HPG–PLA12, HPG–PLA21, HPG–PLA40 and HPG–PLA60 nanoparticles; the release data were fitted to model 3. **b** The release rate of BSA from HPG–PLA12, HPG–PLA21, HPG–PLA40 and HPG–PLA60 nanoparticles

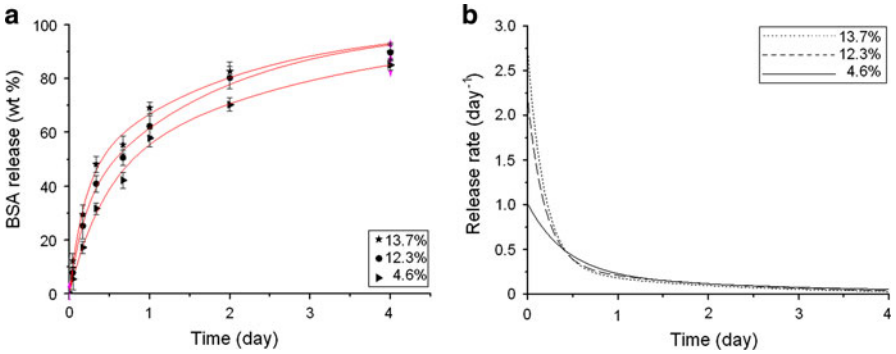

Fig. 9 **a** In vitro release profiles of BSA from HPG–PLA21 nanoparticles with different LC; the release data were fitted to model 3. **b** The release rate of BSA from HPG–PLA21 nanoparticles with different LC

various mechanisms that control protein release, mechanisms such as copolymer relaxation, protein diffusion, protein dissolution or combinations of the above. Concerning the mathematical modeling of BSA release from HPG–PLA nanoparticles, one must identify the most important release phenomenon and neglect the other processes; otherwise the mathematical model would become too complex to use.

Figures 8 and 9 show the cumulative BSA release as a function of time and the corresponding release rates. In all curves a burst effect was observed followed by a slowly continuous release phase. The objective of mathematical analysis is to elucidate the protein release mechanism involved in the release of BSA from the copolymer nanoparticles by fitting obtained data into three models. The criterion for selecting the most appropriate model was based on the adjusted coefficient of determination (R^2_{adjusted}). The parameters are shown in Table 3.

The release data were firstly fitted to the Ritger-Peppas equation ($M_t/M_\infty \leq 60\%$) (Eq. 5), which was often used to describe the drug release behavior from polymeric systems when the mechanism was not well-known or when more

Table 3 Kinetic fitting results of BSA released from nanoparticles with different kinetic models

Material	LC (%)	Ritger–Peppas model			Peppas–Sahlin model			The first-order kinetic model				
		K_{RP}	n	R^2_{adj}	K_1	K_2	R^2_{adj}	a_1	a_2	k_1	k_2	R^2_{adj}
HPG–PLA12	9.1 ± 0.6[a]	0.742	0.491	0.990	0.909	−0.227	0.987	0.462	0.539	5.549	0.524	0.991
HPG–PLA21	4.6 ± 0.9	0.575	0.648	0.968	0.601	−0.083	0.978	0.336	0.663	2.344	0.333	0.992
	12.3 ± 0.7[a]	0.661	0.545	0.969	0.758	−0.150	0.987	0.341	0.662	5.304	0.521	0.994
	13.7 ± 1.2	0.710	0.477	0.964	0.886	−0.216	0.990	0.437	0.555	5.414	0.548	0.989
HPG–PLA40	15.5 ± 1.1[a]	0.550	0.557	0.990	0.621	−0.092	0.988	0.318	0.676	3.614	0.421	0.995
HPG–PLA60	17.8 ± 1.3[a]	0.524	0.658	0.994	0.541	−0.061	0.978	0.301	0.689	1.368	0.199	0.996

[a] 8 mL BSA solution (0.625 mg/mL) was used as the aqueous phase and other conditions were the same as described in Table 2

than one type of release phenomena were involved [43]. All the formulations showed $0.43 < n < 0.85$ (Table 3) after fitting to Eq. 5, which indicated anomalous release mechanism in all cases (non-Fickian kinetics) [24, 44]. The non-Fickian kinetics corresponds to the coupling of diffusion and polymer relaxation. However, in the case of HPG–PLA nanoparticles, it has to be pointed out that the application of the Ritger–Peppas equation can only give limited insight into the exact release mechanism of protein release. The equation is only appropriate in very specific cases. For instance, the protein must be initially homogeneously distributed within the nanoparticles and desorption processes must be negligible. So, it was just an approximate analysis of BSA release mechanism and the information obtained should be viewed with caution.

The relative contribution of BSA diffusion and relaxational contribution to the release mechanism was quantified by fitting the data with Model 2 (Eq. 6) ($M_t/M_\infty \leq 95\%$) [25]. The first term of the right hand side of the equation was the Fickian contribution, *DIF*, while the second term was the relaxational contribution, REL. The ratio of both contributions can be calculated as follows:

$$\mathrm{DIF/REL} = \frac{K_1}{K_2 t^{0.5}} \tag{9}$$

Take the fitting data (K_1 and K_2) of HPG–PLA21 for instant, the ratio (Eq. 9) decreased with the passage of time [45]. It means that the relaxational contribution increased with the lapse of time in the release process. There results indicate the copolymer relaxation makes bigger contribution to the release mechanism when water molecules penetrate into the nanoparticles, especially at the final stage of release profile. However, the ratio (Eq. 9) ranged from 2.5 to 24.8 during the whole process, which suggested that BSA release was still Fickian controlled.

The application of the first-order kinetics is valid for a surface action and those water-soluble drugs releasing from porous matrices [29]. In this work, such a model should be suitable for describing the corresponding experimental data.

$d(M_t/M_\infty)/dt$, which is proportional to the mass of the encapsulated drug, can be described by the following equation [46]:

$$d(M_t/M_\infty)/dt = k(1 - M_t/M_\infty) \quad (10)$$

where M_∞ and M_t are the mass of drug in the nanoparticles at time $t = 0$ and the mass released at time t, respectively, and k is the first-order release constant.After integration, it will become:

$$M_t/M_\infty = 1 - \exp(-kt) \quad (11)$$

Protein-loaded nanoparticles fabricated from nanoprecipitation method entrapped BSA both close to the outer nanoparticles surface and within the protein carriers [10]. BSA on the nanoparticle surface was susceptible to be easily and rapidly released [47]. However, BSA entrapped inside the nanoparticles would display a relative slow release process for the tortuosity and long diffusion path of the protein matrices. As shown in Figs. 8 and 9 (experimental data), the release of BSA apparently consisted of two stages (a relatively fast release profile and followed by a slow one), which could be described by Eq. 7. So, fitting the release data to Eq. 7, the release profiles are obtained as shown in Figs. 8 and 9. k_1 and k_2 were the first-order release rate constants, which reflected the release rate of BSA located on the out layer and entrapped inside the nanoparticles, respectively; a_1 and a_2 meant the percentage of BSA located on the out layer and entrapped inside the nanoparticles, respectively. Quite high R^2_{adjusted} could be obtained with the kinetic model as shown in Table 3. The model seemed to be the most suitable one to describe the experimental data.

The release rate–time curves could be obtained from Eq. 12 expressed as follows:

$$d(M_t/M_\infty)/dt = a_1k_1\exp(-k_1t) + a_2k_2\exp(-k_2t) \quad (12)$$

First, in every case k_1 was considerably greater than k_2, implying that the release rate of BSA on the out layer of nanoparticles was much faster than those inside of the nanoparticles, which was consistent with the experimental results. Second, in every case, as expected, $a_1 + a_2 \approx 1$, this further confirmed the physical interpretation of the two parameters.

At early times (t near 0), $\exp(-kt) \approx 1 - kt$, and Eq. 7 can be expressed as:

$$M_t/M_\infty = a_1(1 - \exp(-k_1t)) + a_2(1 - \exp(-k_2t)) \approx (a_1k_1 + a_2k_2)t \quad (13)$$

This relation could be used to describe the drug release of coated forms [29]. The expression demonstrated the existence of the burst release from BSA close to the outer nanoparticle layer at early times, which was in good agreement with the experimental results.

The theoretical and the experimental data of nanoparticles made with HPG–PLA12, HPG–PLA21, HPG–PLA40, and HPG–PLA60 are shown in Fig. 8. a_1 and k_1 values were found to decrease with an increase in molecular weight, which meant the decrease of BSA percentage located on the out layer of nanoparticles and a slower release rate. In addition, k_2 also decreased with increasing M_n of the copolymers, which would result from an increase of the average particle size from

163 to 287 nm (an increase of diffusion path). Figure 9 shows the release profiles from HPG–PLA21 nanoparticles with different LC. a_1 and k_1 values were found to increase with an increase of LC, which meant the increase of BSA percentage located on the out layer of nanoparticles and a faster release rate. Furthermore, k_2 increased with an increase of LC, which might be due to a shorter BSA diffusion path in the matrices.

Conclusion

HPG–PLA nanoparticles were designed to be applied for a protein delivery system. The results obtained during experimental and mathematical analysis showed that two mechanisms of BSA release, namely protein diffusion and macromolecular relaxation, combined to control the release process. BSA located on the out layer and entrapped inside the nanoparticles jointly governed the overall release profile as evaluated by the first-order kinetic model. The relevant relationship that existed between the characteristics of nanoparticles (copolymer structure and BSA loading capacity) and the release behavior could be exploited to develop unique protein delivery system with exclusively defined release properties.

Acknowledgments This work was supported in part by the National Natural Science Foundation of China (Grant No. 20804021), the Natural Science Foundation of Tianjin (Grant No. 08JCYBJC00300) and the Ph.D. Programs foundation for new teachers of Ministry of Education of China (No. 200800551030).

References

1. Qiu LY, Bae YH (2006) Polymer architecture and drug delivery. Pharm Res 23:1–30
2. Ankola DD, Ravi Kumar MNV, Chiellini F, Solaro R (2009) Multiblock copolymers of lactic acid and ethylene glycol containing periodic side-chain carboxyl groups: synthesis, characterization, and nanoparticle preparation. Macromolecules 42:7388–7395
3. Rieger J, Freichels H, Imberty A, Putaux JL, Delair T, Jérôme C, Velty RA (2009) Polyester nanoparticles presenting mannose residues: toward the development of new vaccine delivery systems combining biodegradability and targeting properties. Biomacromolecules 10:651–657
4. Jiang L, Liu B, Zhang J (2009) Properties of poly(lactic acid)/poly(butylene adipate-co-terephthalate)/nanoparticle ternary composites. Ind Eng Chem Res 48:7594–7602
5. Gou ML, Zheng XL, Men K, Zhang J, Zheng L, Wang XH, Luo F, Zhao YL, Zhao X, Wei YQ, Qian ZY (2009) Poly(ε-caprolactone)/poly(ethylene glycol)/poly(ε-caprolactone) nanoparticles: preparation, characterization, and application in doxorubicin delivery. J Phys Chem B 113:12928–12933
6. Kainthan RK, Janzen J, Levin E, Devine DV, Brooks DE (2006) Biocompatibility testing of branched and linear polyglycidol. Biomacromolecules 7:703–709
7. Sunder A, Hanselmann R, Frey H, Mülhaupt R (1999) Controlled synthesis of hyperbranched polyglycerols by ring-opening multibranching polymerization. Macromolecules 32:4240–4246
8. Adeli M, Haag R (2006) Multiarm star nanocarriers containing a poly(ethylene imine) core and polylactide arms. J Polym Sci Pol Chem 44:5740–5749
9. Gottschalk C, Wolf F, Frey H (2007) Multi-Arm star poly (L-lactide) with hyperbranched polyglycerol core. Macromol Chem Phys 208:1657–1665
10. Gao H, Yang YW, Fan YG, Ma JB (2006) Conjugates of poly(DL-lactic acid) with ethylenediamino or diethylenetriamino bridged bis(β-cyclodextrin)s and their nanoparticles as protein delivery systems. J Control Release 112:301–311

11. Herrmann S, Winter G, Mohl S, Siepmann F, Siepmann J (2007) Mechanisms controlling protein release from lipidic implants: Effects of PEG addition. J Control Release 11:161–168
12. Juliana FP, de Moura Márcia R, Adley FR, Edvani CM (2008) Kinetic Study of bovine serum albumin (BSA) released from alginate-Ca2+/PNIPAAm hydrogels. Macromol Symp 266:108–113
13. Herrmann S, Mohl S, Siepmann F, Siepmann J, Winter G (2007) New insight into the role of polyethylene glycol acting as protein release modifier in lipidic implants. Pharm Res 24:1527–1537
14. Arifin DY, Lee LY, Wang CH (2006) Mathematical modeling and simulation of drug release from microspheres: implications to drug delivery systems. Adv Drug Delivery Rev 58:1274–1325
15. Lin CC, Metters AT (2006) Hydrogels in controlled release formulations: network design and mathematical modeling. Adv Drug Delivery Rev 58:1379–1408
16. Matsumoto J, Nakada Y, Sakurai K, Nakamura T, Takahashi Y (1999) Preparation of nanoparticles consisted of poly(L-lactide)–poly(ethylene glycol)–poly(LL-lactide) and their evaluation in vitro. Int J Pharm 185:93–101
17. Gao X, Zhang X, Wu Z, Zhang X, Wang Z, Li C (2009) Synthesis and physicochemical characterization of a novel amphiphilic polylactic acid-hyperbranched polyglycerol conjugate for protein delivery. J Control Release 140:141–147
18. Barichello JM, Morishita M, Takayama K, Nagai T (1999) Encapsulation of hydrophilic and lipophilic drugs in PLGA nanoparticles by the nanoprecipitation method. Drug Dev Ind Pharm 25:471–476
19. Zhang X, Zhang H, Wu Z, Wang Z, Niu H, Li C (2008) Nasal absorption enhancement of insulin using PEG-grafted chitosan nanoparticles. Eur J Pharm Biopharm 68:526–534
20. Boyer C, Whittaker MR, Chuah K, Liu J, Davis TP (2009) Modulation of the surface charge on polymer-stabilized gold nanoparticles by the application of an external stimulus. Langmuir 26(4):2721–2730
21. Bradford MM (1976) A rapid and sensitive method for the quantitation of microgram quantities of protein utilizing the principle of protein-dye binding. Anal Biochem 72:248–254
22. Richard WK, Robert G, Eric D, Pierre B, Nikolaos AP (1983) Mechanisms of solute release from porous hydrophilic polymers. Int J Phytorem 15:25–35
23. Serra L, Doménech J, Peppas NA (2006) Drug transport mechanisms and release kinetics from molecularly designed poly(acrylic acid-g-ethylene glycol) hydrogels. Biomaterials 27:5440–5451
24. Siepmann J, Peppas NA (2001) Modeling of drug release from delivery systems based on hydroxypropyl methylcellulose (HPMC). Adv Drug Deliver Rev 48:139–157
25. Pitarresi G, Craparo EF, Palumbo FS, Carlisi B, Giammona G (2007) Composite nanoparticles based on hyaluronic acid chemically cross-linked with α,β-polyaspartylhydrazide. Biomacromolecules 8:1890–1898
26. Lewis JL, Dennis A, James C, Nora C (1985) The in vitro development of extended-release solid oral dosage forms. J Pharmacokinet Biopharm 13:493–514
27. Sainsbury EJ, Ashley JJ (1986) Curve-fitting in pharmacokinetics—a comparison between gamma and biexponential fits. Eur J Clin Pharmacol 30:243–244
28. Hiroshi S, Koichi O, Akihiro T, Nobuya H, Shigeo O, Sachio K, Robert VM (2009) Biexponential apparent diffusion coefficients in prostate cancer. Magn Reson Imaging 27:355–359
29. Costa P, Lobo JMS (2001) Modeling and comparison of dissolution profiles. Eur J Pharm Sci 13:123–133
30. Biot C, Bauer H, Schirmer RH, Charvet ED (2004) 5-Substituted tetrazoles as bioisosteres of carboxylic acids. Bioisosterism and mechanistic studies on glutathione reductase inhibitors as antimalarials. J Med Chem 47:5972–5983
31. Nicolaou KC, Snyder SA, Huang X, Simonsen KB, Koumbis AE, Bigot A (2004) Studies toward diazonamide A: initial synthetic forays directed toward the originally proposed structure. J Am Chem Soc 126:10162–10173
32. Kakuchi T, Narumi A, Matsuda T, Miura Y, Sugimoto N, Satoh T, Kaga H (2003) Glycoconjugated polymer. 5. Synthesis and characterization of a seven-arm star polystyrene with a β-cyclodextrin core based on tempomediated living radical polymerization. Macromolecules 36:3914–3920
33. Liu Y, Song Y, Wang H, Zhang HY, Wada T, Inoue Y (2003) Selective binding of steroids by bridged bis(β-cyclodextrin) with 2,2-biquinoline-4,4′-dicarboxylate: fluorescence enhancement induced by guest inclusion. J Org Chem 68:3687–3690
34. Jin X, Zhang X, Wu Z, Teng D, Wang Z, Li C (2009) Amphiphilic random glycopolymer based on phenylboronic acid: synthesis, characterization, and potential as glucose-sensitive matrix. Biomacromolecules 10:1337–1345

35. Peng H, Xiao Y, Mao X, Chen L, Crawford R, Whittaker AK (2009) Amphiphilic triblock copolymers of methoxy-poly(ethylene glycol)-b-poly(L-lactide)-b-poly(L-lysine) for enhancement of osteoblast attachment and growth. Biomacromolecules 10:95–104
36. Zeng JB, Li YD, Li WD, Yang KK, Wang XL, Wang YZ (2009) Synthesis and properties of poly(ester urethane)s consisting of poly(L-lactic acid) and poly(ethylene succinate) segments. Ind Eng Chem Res 48:1706–1711
37. Agarwal M, Koelling KW, Chalmers JJ (1998) Characterization of the degradation of polylactic acid polymer in a solid substrate environment. Biotechnol Prog 14:517–526
38. Gao H, Wang YN, Fan YG, Ma JB (2005) Synthesis of a biodegradable tadpole-shaped polymer via the coupling reaction of polylactide onto mono(6-(2 aminoethyl)amino-6-deoxy)-h-cyclodextrin and its properties as the new carrier of protein delivery system. J Control Release 107:158–173
39. Crotts G, Sah H, Park TG (1997) Adsorption determines in vitro protein release rate from biodegradable microspheres: quantitative analysis of surface area during degradation. J Control Release 47:101–111
40. Anon (2000) United States Pharmacopeia. In: Biological reactivity tests in vitro, 24th revision. United States Pharmacopeial Convention, Inc., Rockville, Maryland, pp 1813–1831
41. Molina I, Li S, Martinez MB, Vert M (2001) Protein release from physically crosslinked hydrogels of the PLA/PEO/PLA triblock copolymer-type. Biomaterials 22:363–369
42. Eijsink VG, Gåseidnes S, Borchert TV, van den BB (2006) Directed evolution of enzyme stability, Biomol Eng 22:21–30
43. Sriamornsak P, Thirawong N, Korkerd K (2007) Swelling, erosion and release behavior of alginate-based matrix tablets. Eur J Pharm Biopharm 66:435–450
44. Stulzer HK, Lacerda L, Tagliari MP, Silva MAS, Fávere VT, Laranjeira MCM (2008) Synthesis and characterization of cross-linked malonylchitosan microspheres for controlled release of acyclovir. Carbohydr Polym 73:490–497
45. Munday DL, Cox PJ (2000) Compressed xanthan and karaya gum matrices: hydration, erosion and drug release mechanisms. Int J Pharm 203:179–192
46. Zhou W, Feijen J (2008) Biodegradable polymersomes for controlled drug release. J Control Release 132:e35–e36
47. Ubrich N, Bouillot P, Pellerin C, Hoffman M, Maincent P (2004) Preparation and characterization of propranolol hydrochloride nanoparticles: a comparative study. J Control Release 97:291–300